Published in "Journal of Materials Chemistry 17(13): 1262-1267, 2007"
which should be cited to refer to this work.

Controlling the lateral aggregation of perfluoroalkylated hexa-*peri*-hexabenzocoronenes†

Olivier F. Aebischer,[a] Annina Aebischer,[b] Bertrand Donnio,[c] Bassam Alameddine,[d] Massoud Dadras,[e] Hans-Ulrich Güdel,[b] Daniel Guillon[c] and Titus A. Jenny*[a]

The investigation of two hexa-*peri*-hexabenzocoronene (HBC) derivatives carrying linear or branched perfluoroalkylated side chains is reported. Polycondensed aromatic hydrocarbons (PAH) such as HBC derivatives are well known to self-organize to form highly ordered monomolecular stacks, which in turn show a concentration- and solvent-dependent lateral aggregation. However, possible applications of self-assembled HBC derivatives require linear, laterally non-aggregated columnar structures. According to powder X-ray diffraction (XRD) and differential scanning calorimetry (DSC), HBC derivatives with linear perfluoroalkylated side chains show liquid crystalline (LC) properties whereas those with branched perfluoroalkylated side chains have an amorphous structure. The stacking behaviour and the lateral aggregation are found to be greatly influenced by changes in the medium, as shown by fluorescence spectroscopy and cryo-scanning electron microscopy (cryo-SEM).

Introduction

Polycondensed aromatic hydrocarbons (PAH) have been the focus of intensive investigations over the past decade due to their pronounced tendency to form columnar ordered supramolecular architectures by non-covalent bonding such as π–π interactions.[1] PAHs, which can be regarded as two-dimensional subsections of graphite, are well defined nanoobjects.[2–5] They are of particular interest because they form linear, laterally insulated conducting structures, so called nanowires, with a potential application in the field of electronic devices.[6–8] From this perspective, many different PAHs have been investigated over the past few years, such as triphenylenes,[9,10] perylenes,[11] corannulenes,[12] polyphenylfluorenes[13] as well as hexa-*peri*-hexabenzocoronenes (HBC)[14] and its larger analogues.[15] In addition, discrete nanotubular objects formed by the self-assembly of HBC amphiphiles were recently reported in the literature.[16,17] From a synthetic point of view, HBCs are the most versatile representatives, as they are easily made with a large variety of different substituents at their periphery.[18–20] Highly symmetric HBC derivatives carrying appropriate side chains excel not only with their liquid-crystalline properties, but also with their outstanding thermal stability. In addition, HBC derivatives display a charge-carrier mobility in the bulk,[21] which is much higher than that of smaller discotic molecules, such as triphenylene derivatives, because they form highly ordered columnar structures in the discotic liquid-crystalline phase.[22]

In alkylated HBC derivatives, these columns have been shown to aggregate to form two- or three-dimensional geometries.[23] Many attempts were made to prevent this lateral aggregation and to prepare monostranded stacks. The lateral aggregation is reduced on dilution but this also enhances the disassembly of the strands.[24] The aggregation of HBC-based materials has been intensively investigated by different methods such as X-ray diffraction, scanning probe microscopy, angle-resolved ultraviolet photoelectron spectroscopy, solid-state NMR, ^{1}H-NMR, vapour pressure osmometry and optical spectroscopy.[25–28]

In an effort to reduce lateral aggregation without altering the desired π–π-stacking, we synthesized HBCs with perfluoroalkylated side chains. Surprisingly, aliphatic spacers, placed between the HBC core and the perfluoroalkylated side chain for synthetic reasons, turned out to be crucial for hindering lateral aggregation.[29,30] As compared to HBCs with purely aliphatic side chains, the new mixed alkyl/perfluoroalkyl HBCs showed less aggregation between individual columnar structures in solution.

Furthermore, the phase-transition temperatures observed in DSC measurements for such compounds were found to be much higher than for their purely aliphatic analogues.[31] We explain these findings by the formation of much longer columnar structures, which compensate for the reduced lateral interactions.[29]

[a]*Department of Chemistry, University of Fribourg, chemin du Musée 9, 1700 Fribourg, Switzerland. E-mail: titus.jenny@unifr.ch; Fax: +41 26 300 9739; Tel: +41 26 300 8778*
[b]*Department of Chemistry and Biochemistry, University of Bern, Feiestrasse 3, 3000 Bern 9, Switzerland. E-mail: guedel@iac.unibe.ch; Fax: +41 31 631 4399; Tel: +41 31 631 4249*
[c]*Institut de Physique et Chimie des Matériaux de Strasbourg (IPCMS), Groupe des Matériaux Organiques (GMO), UMR 7504, CNRS/ Université Louis Pasteur, 23, rue du Loess, BP 43, 670334 Strasbourg Cedex 2, France. E-mail: bdonnio@ipcms.u-strasbg.fr; Fax: +33 38 810 7246; Tel: +33 38 810 7157*
[d]*Department of Chemistry, University of Balamand, Tripoli, Lebanon. E-mail: balameddine@hotmail.com; Fax: +961 166 3885; Tel: +961 693 0250*
[e]*Service for Microscopy and Nanoscopy, IMT, University of Neuchâtel, 2007 Neuchâtel, Switzerland. E-mail: massoud.dadras@unine.ch; Fax: +41 32 720 5711; Tel: +41 32 720 5248*

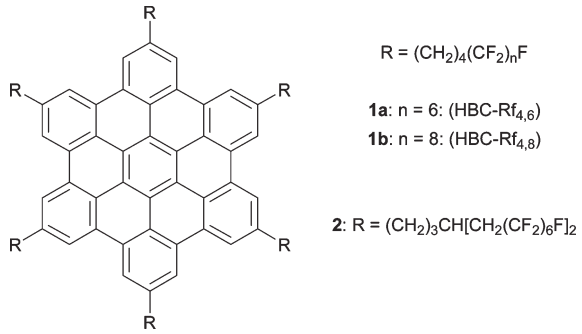

Fig. 1 Structure of HBC derivatives **1a**, **1b** and **2**.

All the investigation techniques mentioned above showed, however, that the formation of single stranded columnar assemblies was invariably accompanied by some lateral aggregation. However, by modifying the side chain geometry,[32] tuning the fluorination level and by varying the solvent we intended to gain some control over this undesirable feature.

We report herein our results on two different perfluoroalkylated HBC derivatives (Fig. 1): one with linear side chains, HBC–$[(CH_2)_4(CF_2)_6F]_6$ (**1a**), and one with branched side chains, HBC–$[(CH_2)_3CH\{(CH_2CF_2)_6F\}_2]_6$ (**2**). The alkylated section in the periphery not only insulates the core structure from the electron withdrawing effect of the perfluorinated part at the end of the chain, which is detrimental in the synthesis of the HBC core, but moreover, endows the molecule with a certain flexibility, as perfluoroalkylated chains are known to be rather stiff.[33] Preliminary investigations had shown that spacers shorter than four hydrogenated carbon atoms led to decreased solubility in a range of solvents, whereas longer spacers reduced the desired effect of the fluorinated part.[29] On the other hand, small changes in the number of perfluorinated carbons, as for instance between HBC–$Rf_{4,6}$ (**1a**) and HBC–$Rf_{4,8}$ (**1b**), led to tremendously decreased solubility, whereas the columnar self-assembly properties did not change dramatically. As the solubility of the HBC derivatives is critical for their purification, **1a** was chosen for a more detailed investigation, which is now reported. In order to further increase the fluorine coating of the HBC stack, a second HBC (**2**) derivative carrying branched side chains was designed. The branched six-carbon aliphatic spacer carries two perfluorohexyl parts, which decreases the alkyl/perfluoroalkyl ratio enormously without affecting the solubility.

Results and discussion

Properties and characterization

The synthesis of **1a**, **1b** and **2** has been described elsewhere.[29,34] It must be pointed out, however, that all three fluorinated HBC derivatives are only sparingly soluble in common organic solvents, such as acetone, carbon disulfide, dichloromethane, ether, pentane, THF and toluene, which seriously hampers the characterization of new compounds by NMR spectroscopy.

Only highly halogenated aromatic solvents, such as 1,2,4-trichlorobenzene (TCB), benzotrifluoride (BTF) and hexafluorobenzene (HFB), were able to solubilize our fluorinated HBC derivatives. HBC **2**, with its branched side chains, was in general more soluble than the linear ones, except in TCB where it was completely insoluble. Furthermore, **2** is to our knowledge the first perfluoroalkylated HBC derivative which is not obtained as a powder but as a completely amorphous, highly viscous glass-like substance. A similar property was reported so far only for an HBC derivative with six long $C_{20}H_{41}$ side chains.[35]

The ^{1}H-NMR spectra of **1a** and **2** in hexafluorobenzene were not very well-resolved. Mass spectrometry remained, therefore, the only reliable technique to prove the presence of the desired molecules provided that the reported solvent-free MALDI-ICR conditions were applied with DCTB or TCNQ as the matrix.[36] In our experience, MALDI-ICR of these compounds was found to be highly sensitive to the purity of the HBC derivatives, in that the ion intensity rapidly decreases in the presence of tiny amounts of impurities. The MALDI-ICR spectra of HBC **1a** and **2** are shown in Fig. 2.

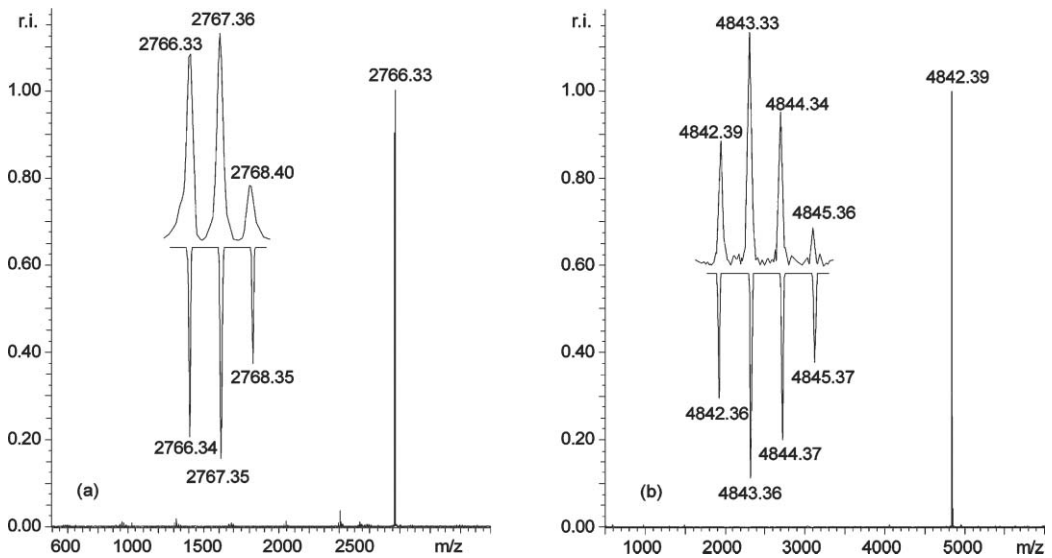

Fig. 2 (a) MADLI-ICR spectrum of HBC **1a**, inset: measured (up) and calculated isotopic pattern (down), calculated for $C_{102}H_{60}F_{78}$. (b) MADLI-ICR spectrum of HBC **2**, inset: measured (up) and calculated isotopic pattern (down), calculated for $C_{150}H_{78}F_{156}$.

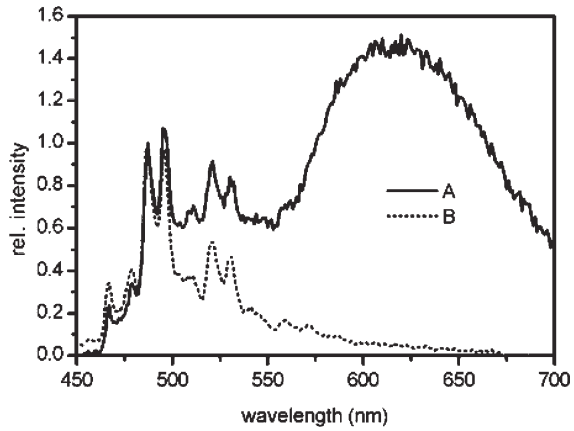

Fig. 3 Fluorescence spectra (λ_{ex} = 360 nm) of HBC **1a** in BTF at various concentrations: (A) 10^{-3} M and (B) 10^{-5} M. The fluorescence spectra are arbitrarily scaled at 487 nm.

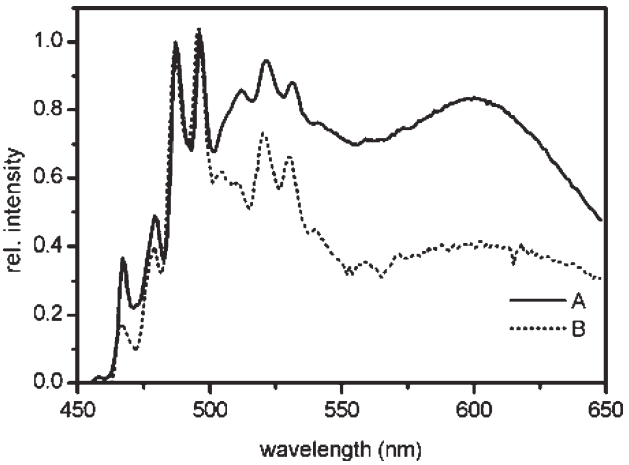

Fig. 4 Fluorescence spectra (λ_{ex} = 360 nm) of HBC **1a** at 10^{-4} M in BTF: (A) room temperature (25 °C) and (B) 60 °C. The fluorescence spectra are arbitrarily scaled at 487 nm.

Fluorescence spectroscopy

Fluorescence spectroscopy was performed with solutions of HBC **1a** and **2** at concentrations ranging from 10^{-3} to 10^{-10} M in TCB, BTF and HFB. Fig. 3 shows the fluorescence spectra of HBC **1a** in HFB at two concentrations. Below 10^{-4} M, only the resolved fluorescence features of monomeric HBC could be observed.[37] By increasing the concentration to 10^{-3} M, a broad red-shifted band appears, which can be attributed to aggregated HBC architectures. By comparing the fluorescence data with cryo-SEM micrographs of solutions of the same concentrations,[38] we conclude that around 10^{-4} M monomeric HBCs are the predominant species together with monostranded HBC columns, while above 10^{-4} M larger laterally aggregated architectures coexist with few thinner filaments. The variation of the concentration has the expected effect: at high concentrations ($\geqslant 10^{-3}$ M), large structures are dominant whereas on lowering the concentration (around 10^{-4} M), lateral aggregation first decreases to yield mostly monostranded HBC stacks, which disassemble into their molecular components on further lowering of the concentration ($\leqslant 10^{-5}$ M).

Fig. 4 shows the fluorescence spectra of a 10^{-4} M solution of HBC **1a** in BTF at two different temperatures. The room temperature spectrum (Fig. 4A) reveals the presence of monomeric HBC moieties in combination with the red-shifted aggregates. By increasing the temperature to 60 °C (Fig. 4B), the intensity of the broad band at around 600 nm decreases significantly. The intensity of the low energy part of the spectrum may, therefore, be affected either by variation of the concentration or of the temperature, in a process that is fully reversible.

Fig. 5 shows the fluorescence spectra of HBC **1a** and **2** at 10^{-4} M in three different solvents. As expected, **1a** shows no traces of monomeric HBC in TCB (Fig. 5A), *i.e.* at this concentration only aggregated HBC structures are present. Two factors are responsible for this behaviour: *i*) the low solubility of **1a**, which favours aggregation; and *ii*) the low tendency of π–π complexation of TCB and HBCs, which allows the formation of very extended structures. Accordingly, in BTF solutions a dynamic equilibrium between aggregated and monomeric **1a** is observed (Fig. 5B). On the other hand, the fluorescence spectrum of **1a** in HFB (Fig. 5C) shows almost exclusively HBC monomer emission. Again, two reasons might be responsible for this observation: *i*) the high solubility of the monomer; and *ii*) the high end-capping tendency of HFB, which favours short aggregated structures. In addition, the luminescence intensity is reduced by two orders of magnitude in this solvent, as compared to BTF.

HBC **2** (Fig. 5D), with its branched lateral chains, shows a completely different behaviour; even at concentrations of 10^{-4} M in BTF, no broad band around 600 nm is observed. This implies that even at this fairly high concentration most of the material is monomeric.

In TCB, **2** was completely insoluble and formed a suspension which prevented the collection of meaningful fluorescence data. In HFB, the fine structure of the fluorescence is washed out, probably due to aggregate formation between HBC **2** and the solvent.

Cryo-SEM investigations

Therefore, we decided to investigate our samples by cryo-SEM, a technique favoured by biologists to investigate cryogenated biological cell samples.[39]

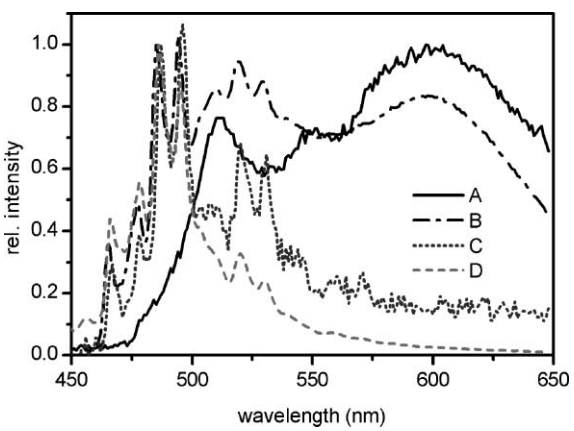

Fig. 5 Fluorescence spectra (λ_{ex} = 360 nm) of 10^{-4} M solutions of HBC **1a** in: (A) TCB, (B) BTF and (C) HFB, and of HBC **2**, (D) in BTF. The fluorescence spectra are arbitrarily scaled at 487 nm.

Our self-assembled HBC structures show a dynamic equilibrium of various aggregated HBC architectures, which is very sensitive to concentration variations, such as those occurring during spin coating. In contrast, upon shock freezing in liquid nitrogen, the formed aggregates are preserved. By partially subliming the solvent at −95 °C and 10^{-4}–10^{-5} mbar directly in the cryo-prechamber, the pre-existing architectures are exposed on the recoiling frozen solvent surface. In order to render the target conducting, a platinum coating of about 20 nm has to be applied.[30]

Observing the samples prepared from 10^{-4} M solutions led to the micrographs depicted in Fig. 6. HBC **1a** in TCB (micrographs A_1 and A_2) reveals the presence of very long structures of rectangular cross-section, presumably formed by lateral aggregation of HBC fibres into sheets, which stack to form piles. The remarkable length (20 μm on average) of these structures corroborates the assumption of a low π–π complexing tendency of TCB, leading to no end-capping. The typical cross-section of these flat structures is about 100 nm × 250 nm, which corresponds to approximately 2000 laterally-aggregated HBC filaments. However, the samples obtained form BTF solutions result in structures (micrographs B_1 and B_2) showing a much wider range of different forms, as compared to those obtained from TCB solutions. Large bundles of laterally-aggregated HBC columns with an average length of about 20 μm and a cross-section of up to 500 × 200 nm are observed. In addition, the previously observed (A_1 and A_2) completely regular fibers in TCB show several splittings into smaller strands that rapidly taper off in samples obtained from BTF solutions. In contrast, in preparations from HFB solutions of the same concentration, the compound only shows thin regular aggregated structures with a cross-section of 35 nm and a typical length of 200 nm, 100 times shorter than in the other solvents (Fig. 6C). The observed uniform cross-section of 35 nm indicates the presence of monostranded HBC stacks; as for the observation in cryo-SEM, a platinum coating of approximately 20 nm is applied. The observed short columns corroborate our assumption of pronounced π–π complexation by this solvent, resulting in an efficient end-capping of the columns. Finally for HBC **2**, with its branched side chains, only a few thin structures with a cross-section of approximately 40 nm and a typical length of 5 μm are found in BTF solutions (Fig. 6D). Furthermore, no laterally-aggregated structures can be observed for this derivative.

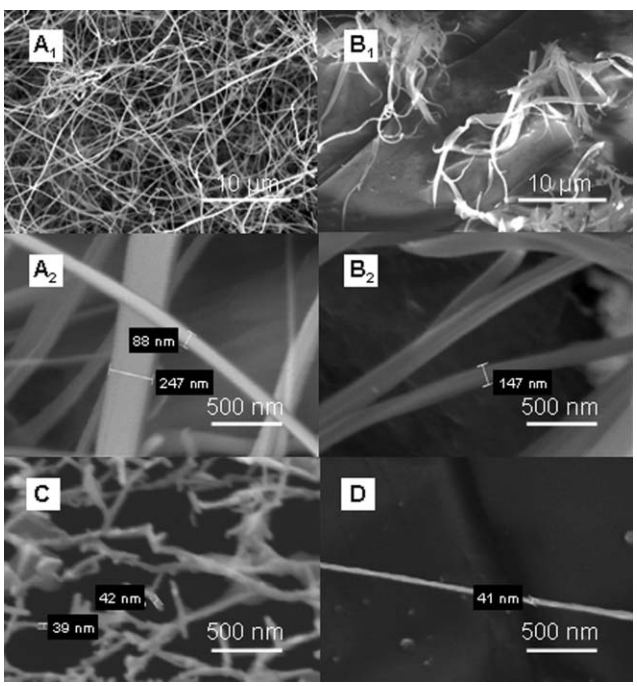

Fig. 6 Cryo-SEM micrographs obtained from 10^{-4} M BTF solutions of HBC **1a** in: (A_1 and A_2) TCB, (B_1 and B_2) BTF and (C) HFB, and of (D) HBC **2** in BTF.

DSC and X-ray investigations

The thermal behaviour of both HBC derivatives was analyzed by DSC and XRD. Whereas **2** is obtained as an amorphous solid, which is directly transformed to the isotropic liquid-phase upon heating (without a well-defined melting point), **1a** is found to exhibit a liquid-crystalline mesophase, after several crystal-to-crystal phase transitions (Cr_1, Cr_2, Cr_3, DSC in the ESI†). By both DSC and XRD techniques, the following thermal sequence could be determined: Cr_1 103.35 °C Cr_2 155.85 °C Cr_3 194.1 °C Col_h;no isotropization temperature could be given, as the isotropic liquid was still not reached at 250 °C. At 200 °C, the XRD pattern exhibits several sharp small-angle reflections, with spacings in a ratio of $1 : \sqrt{3} : \sqrt{4} : \sqrt{7} : \sqrt{12} : \sqrt{13}$, respectively (see Fig. 7). These reflections are readily assigned as the (10), (11), (20), (21), (22), and (31) of a hexagonal 2D lattice with a = 31.4 Å (at T = 200 °C, see Table 1). A broad halo (h_{ch}) and another sharp signal (h_0) are observed in the wide-angle part, at 5.65 and 3.5 Å, corresponding to the liquid-like order of the molten fluorinated chains, and the stacking of the flat molecular cores, respectively.

Knowledge of the columnar cross-section (S, *cf.* Table 1) and the stacking periodicity (h_0) along the molecular disc normal permits understanding of the molecular packing inside the columns (Fig. 8).[40,41] For instance, one can deduce the intra-columnar repeating periodicity along the columnar axis, h, from the columnar cross-section, S, obtained directly from the X-ray diffraction data (see Table 1), and the molecular

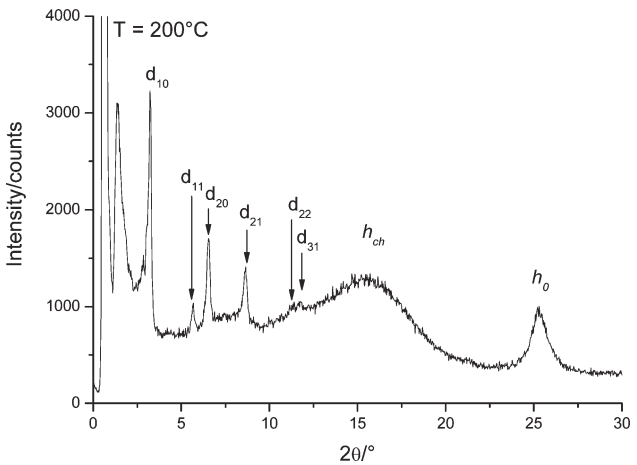

Fig. 7 XRD pattern of HBC **1a** at 200 °C.

Table 1 XRD parameters of HBC **1a**

d_{exp}/Å [a]	[hk] [b]	Intensity[c]	d_{theo}/Å [a,d]	Parameters [d,e]
27.25	10	VS	27.2	a = 31.4 Å;
15.75	11	S	15.7	S = 854.3 Å^2;
13.55	20	VS	13.6	V_{mol} = 3100 Å^3;
10.3	21	S	10.3	h = 3.6 Å
7.85	22	M	7.85	
7.55	31	M	7.55	
5.65	h_{ch}	br	Chains	
3.5	h_0	sh	Stacking	

[a] d_{exp} and d_{theo} are the experimentally measured and theoretical diffraction spacings at 200 °C. The distances are given in Å. [b] [hk] are the indexation of the reflections, and h_0 and h_{ch} are the short-range periodicities determined by XRD, corresponding to the molecular stacking distance (h_0) and to the liquid-like order of the molten chains (h_{ch}), respectively. [c] VS = very strong, S = strong, M = medium, and br and sh = broad and sharp (diffuse) reflections, respectively. [d] d_{theor} and the lattice parameter a are deduced from the following mathematical expressions: $<d_{10}> = 1/N_{hk}[\Sigma d_{hk} \times (h^2 + k^2 + hk)^{1/2}]$ where N_{hk} is the number of hk reflections and $a = 2<d_{10}>/\sqrt{3}$. [e] Col_h = hexagonal columnar phase, Cr_i = crystalline solids, I = isotropic liquid. S = lattice area ($S = a^2\sqrt{3}/2$). V_{mol} = molecular volume ($V_{mol} = V_{HBC} + 6(nV_{CH2} + mV_{CF2})$, where V_{HBC} = 650, $V_{CH2} = 26.5616 + 0.02023T$, and $V_{CF2} = 40.815 + 0.03318T$), h = intracolumnar repeating distance (deduced directly from the measured molecular volume and the columnar cross-section according to $h = V_{mol}/S$).

volume (V_{mol}), which are analytically linked through the relationship $h \times S = N \times V_{mol}$, where N is the number of molecules (aggregation number) within this fraction of columns;[40] in this case, N is chosen to be equal to 1 as the molecule is disc-like. The comparison of h and h_0 is very informative as it can tell us about the various possible organizations of the disc-like molecules within the columns. Thus, for N = 1, an intramolecular stacking of 3.6 Å is determined ($h = V_{mol}/S$), nearly identical to the stacking periodicity within the column (h_0 = 3.5 Å) measured by XRD, indicating that the molecules are stacked (almost) perpendicular (not tilted) with respect to the columnar axis. In order to accommodate the cross-sections of the fluorinated segments with the periodicity between the aromatic cores, the molecules likely stack in an alternating fashion (rotation of *ca.* 30°), the flexible aliphatic spacer allowing the bulky fluorinated chains to expand out of the crown to fill the available volume. This dense packing model of the complex into columns is supported by molecular dynamics simulations.

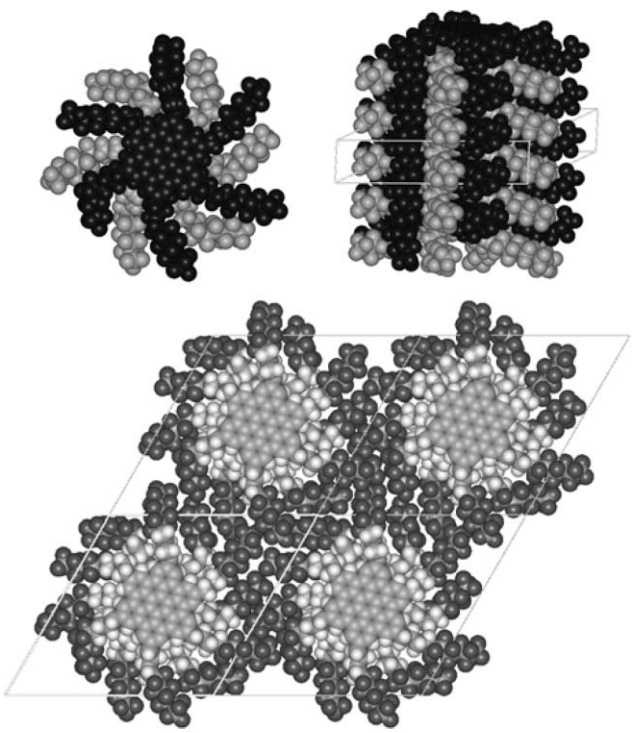

Fig. 8 Top: view of the stacking of neighbouring molecules (left), and side view of the stacking within the column (right). Bottom: snapshot showing the molecular self-assembling of **1a** into the hexagonal lattice of the Col_h phases (polar central core in grey, aliphatic spacers in light grey, fluorinated segments in dark grey. Left: top view. Right: side view.

For this experiment, a periodic molecular model is built from experimental X-ray data, though it is convenient to consider a slice thickness of 14.0 Å (4 × 3.5 Å, corresponding to four stacked molecules). The result of these calculations evidences a good space-filling of the available volume as well as the enhancement of the micro segregation over the entire simulation experiment time, contributing to the cohesion of the columnar structure. The surface area of the discs stacked in a flat conformation is fully compatible with the cross-section of the hexagonal lattice. This model of the packing of **1a** can be used to explain the absence of mesomorphism of **2**, as the chains in this case are too bulky they cannot be accommodated within the cross-sections of the HBC cores, clearly supporting that both the disc–disc interactions and microsegregation are needed to observe mesomorphism.

Experimental

MALDI-ICR spectra were measured on a Bruker 4.7 T BioAPEX II FT/ICR spectrometer using a 337 nm nitrogen laser and *trans*-2-[3-(4-*t*-butyl(phenyl)-2-methyl-2-propenylidene]malonitrile (DCTB) as matrix. As a cryo-SEM system, a Gatan ALTO 2500 installed on a Philips XL30 ESEM FEG microscope was used.

Fluorescence spectra were measured on a Spex-Fluorolog-3-system.

The XRD patterns were obtained with two different experimental set-ups. In all cases, a linear monochromatic CuKα_1 beam (λ = 1.5405 Å) was obtained using a sealed-tube generator (900 W) equipped with a bent quartz monochromator. In the first set, the transmission Guinier geometry was used, whereas a Debye–Scherrer-like geometry was used in the second experimental set-up. In all cases, the crude powder was filled in Lindemann capillaries of 1 mm diameter and 10 μm wall thickness. An initial set of diffraction patterns was recorded on an image plate; periodicities up to 80 Å can be measured, and the sample temperature controlled to within ±0.3 °C from 20 to 350 °C. The second set of diffraction patterns was recorded with a curved Inel CPS 120 counter gas-filled detector linked to a data acquisition computer; periodicities up to 60 Å can be measured, and the sample temperature controlled to within ±0.05 °C from 20 to 200 °C. In each case, exposure times were varied from 1 to 24 h.

The molecular modelling calculations were performed on an SGI Origin 200 4 CPU computer and on an SGI Octane2 workstation using the DISCOVER 3 molecular mechanics package from Accelrys with the pcff force field.

Conclusions

In conclusion, the self-aggregation behaviour of two different HBC derivatives carrying linear (**1a**) or branched (**2**) perfluoroalkylated side chains was investigated by fluorescence spectroscopy, cryo-SEM and XRD measurements. It was shown that the lateral aggregation of HBC **1a** and **2** depends on the nature of the solvent, the concentration and the temperature. Moreover, lateral aggregation is most effectively controlled by side chain engineering, *i.e.* the use of sterically more demanding chains.

Acknowledgements

BD and DG acknowledge the CNRS and the Universtity Louis Pasteur for funding, and thank Dr Cyril Bourgogne and Dr Benoit Heinrich for the modelling and DSC experiments.

References

1 A. J. Berresheim, M. Müller and K. Müllen, *Chem. Rev.*, 1999, **99**, 1747.
2 E. Clar, *Aromatische Kohlenwasserstoffe: Polycyclische Systeme*, Springer, Berlin/Göttingen/Heidelberg, 1952.
3 E. Clar, *The Aromatic Sextet*, John Wiley, London, 1972.
4 G. M. Whitesides and B. Grzybowski, *Science*, 2002, **295**, 2418.
5 O. Ikkala and G. ten Brinke, *Science*, 2002, **295**, 2407.
6 Z. N. Bao, A. J. Lovinger and A. Dodabalapur, *Adv. Mater.*, 1997, **9**, 42.
7 N. Boden, R. J. Bushby, J. Clements, B. Movaghar, K. J. Donovan and T. Kreouzis, *Phys. Rev. B*, 1995, **52**, 13274.
8 R. E. Martin and F. Diederich, *Angew. Chem., Int. Ed.*, 1999, **38**, 1350.
9 S. Kumar, *Liq. Cryst.*, 2005, **32**, 1089.
10 S. Kumar, *Liq. Cryst.*, 2004, **31**, 1037.
11 U. Rohr, P. Schlichting, A. Böhm, M. Gross, K. Meerholz, C. Bräuchle and K. Müllen, *Angew. Chem., Int. Ed.*, 1998, **37**(10), 1434.
12 L. T. Scott, P.-C. Cheng, M. M. Hashemi, M. S. Bratcher, D. T. Meyer and H. B. Warren, *J. Am. Chem. Soc.*, 1997, **119**, 10963.
13 L. Tong, H. Lau, D. M. Ho and R. A. Pascal, *J. Am. Chem. Soc.*, 1998, **120**, 6000.
14 M. D. Watson, A. Fechtenkötter and K. Müllen, *Chem. Rev.*, 2001, **101**, 1267.
15 F. Dötz, J. D. Brand, S. Ito, L. Gherghel and K. Müllen, *J. Am. Chem. Soc.*, 2000, **122**, 7707.
16 J. P. Hill, W. Jin, A. Kosaka, T. Fukushima, H. Ichihara, T. Shimomura, K. Ito, T. Hashizume, N. Ishii and T. Aida, *Science*, 2004, **304**, 1481.
17 W. Jin, T. Fukushima, A. Kosaka, M. Niki, N. Ishii and T. Aida, *J. Am. Chem. Soc.*, 2005, **127**, 8284.
18 M. G. Debije, J. Piris, M. P. de Haas, J. M. Warman, Z. Tomovic, C. D. Simpson, M. D. Watson and K. Müllen, *J. Am. Chem. Soc.*, 2004, **126**, 4641.
19 B. J. Spraul, S. Suresh, S. Glaser, D. Perahia, J. Ballato and D. W. Smith, *J. Am. Chem. Soc.*, 2004, **126**, 12772.
20 J. M. Warman, J. Piris, W. Pisula, M. Kastler, D. Wasserfallen and K. Müllen, *J. Am. Chem. Soc.*, 2005, **127**, 14257.
21 A. M. van de Craats, J. M. Warman, K. Müllen, Y. Geerts and J. D. Brand, *Adv. Mater.*, 1998, **10**, 36.
22 P. Herwig, C. W. Kayser, K. Müllen and H. W. Spiess, *Adv. Mater.*, 1996, **8**, 510.
23 W. Pisula, A. Menon, M. Stepputat, I. Lieberwirth, U. Kolb, A. Tracz, H. Sirringhaus, T. Pakula and K. Müllen, *Adv. Mater.*, 2005, **17**, 684.
24 M. Kastler, W. Pisula, D. Wasserfallen, T. Pakula and K. Müllen, *J. Am. Chem. Soc.*, 2005, **127**, 4286.
25 I. Fischbach, T. Pakula, P. Minkin, A. Fechtenköter, K. Müllen, H. W. Spiess and K. Saalwächter, *J. Phys. Chem. B*, 2002, **106**, 6408.
26 N. Tchebotareva, X. Yin, M. D. Watson, P. Samori, J. P. Rabe and K. Müllen, *J. Am. Chem. Soc.*, 2003, **125**, 9734.
27 R. Friedlein, X. Crispin, C. D. Simpson, M. D. Watson, F. Jäckel, W. Osikowicz, S. Marciniak, M. P. de Jong, P. Samori, S. K. M. Jönsson, M. Fahlman, K. Müllen, J. P. Rabe and W. R. Salaneck, *Phys. Rev. B*, 2003, **68**, 195414.
28 J. Wu, A. Fechtenkötter, J. Gauss, M. D. Watson, M. Kaster, C. Fechtenkötter, M. Wagner and K. Müllen, *J. Am. Chem. Soc.*, 2004, **126**, 11311.
29 B. Alameddine, O. F. Aebischer, W. Amrein, B. Donnio, R. Deschenaux, D. Guillon, C. Savary, D. Scanu, O. Scheidegger and T. A. Jenny, *Chem. Mater.*, 2005, **17**, 4798.
30 O. F. Aebischer, A. Aebischer, P. Tondo, B. Alameddine, M. Dadras, H. U. Güdel and T. A. Jenny, *Chem. Commun.*, 2006, 4221–4223.
31 S. Ito, M. Wehmeier, J. D. Brand, C. Kübel, R. Epsch, J. P. Rabe and K. Müllen, *Chem.–Eur. J.*, 2000, **6**, 4327.
32 K. Balakrishnan, A. Datar, T. Naddo, J. Huang, R. Oitker, M. Yen, J. Zhao and L. Zang, *J. Am. Chem. Soc.*, 2006, **128**, 7390.
33 D. F. Eaton and B. E. Smart, *J. Am. Chem. Soc.*, 1990, **112**, 2821.
34 O. F. Aebischer, P. Tondo, B. Alameddine and T. A. Jenny, *Synthesis*, 2006, **17**, 2891.
35 C.-Y. Liu, A. Fechtenkötter, M. D. Watson, K. Müllen and A. J. Bard, *Chem. Mater.*, 2003, **15**, 124.
36 S. Trimpin, A. Rouhanipour, R. Az, H. J. Räder and K. Müllen, *Rapid Commun. Mass Spectrom.*, 2001, **15**, 1364.
37 Z. Wang, Z. Tomovic, M. Kastler, R. Pretsch, F. Negri, V. Enkelmann and K. Müllen, *J. Am. Chem. Soc.*, 2004, **126**, 7794.
38 Characteristic cryo-SEM micrographs are shown in the ESI†.
39 P. Echlin, *Low-Temperature Microscopy and Analysis*, Plenum Press, New York, 1992.
40 D. Guillon, *Struct. Bonding*, 1999, **95**, 41.
41 F. Morale, R. W. Date, D. Guillon, D. W. Bruce, R. L. Finn, C. Wilson, A. J. Blake, M. Schröder and B. Donnio, *Chem.–Eur. J.*, 2003, **9**, 2484.